pubs.acs.org/Biomac

Article

# Cellulose Nanofibers for Encapsulation and Pluripotency Preservation in the Early Development of Embryonic Stem Cells

Rupambika Das and Javier G. Fernandez*

Cite This: *Biomacromolecules* 2020, 21, 4814–4822

Read Online

ACCESS | Metrics & More | Article Recommendations | Supporting Information

**ABSTRACT:** Materials for three-dimensional cultures aim to reproduce the function of the extracellular matrix, enabling cell adhesion and growth by remodeling the environment. However, embryonic stem cells (ESCs) must develop in environments that prevent adhesion and preserve their pluripotency. In this study, we used cellulose nanofiber hydrogels to mimic the developing conditions required for ESCs. These plant-based hydrogels are simultaneously biocompatible and exogenous to mammalian cells, preventing remodeling and attachment. The storage modulus of these hydrogels could be fine-tuned by varying the degree of oxidation to enable selective degradation. The ESCs proliferated in the artificial environment, forming increasingly large embryoid bodies for 15 days. Unlike traditional cultures in which ESCs begin differentiating upon the removal of the chemical inhibition, the expression of pluripotency markers in the ESC population remained high for the entire two weeks. Cellulase from *Trichoderma reesei* was used to retrieve the ESC cultures selectively. The proposed unique system is a prospective model with which to study the early development of embryonic cells, as well as a nonchemical method of preserving undifferentiated populations of ESCs.

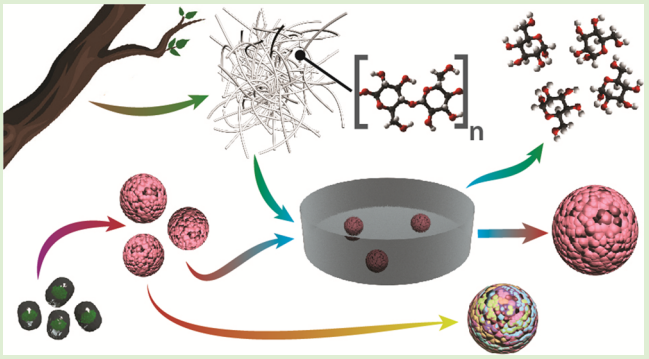

## INTRODUCTION

Three-dimensional (3D) cell culture systems emerged two decades ago in an attempt to overcome the limitations of traditional two-dimensional (2D) culture systems in terms of reproducing physiological phenomena.[1,2] Most 3D culture systems aim to provide a controlled environment to mimic the physiological conditions of a targeted tissue so that the cellular behavior and resulting observations are as close as possible to the *in vivo* counterpart. Mammalian cells natively develop in 3D microenvironments defined by the characteristics of the extracellular matrix (ECM).[3,4] The native ECM is composed of macromolecules, such as fibrin, collagen, and laminin, which form the backbone of the cells and provide them with biochemical cues for propagation and further development.[5,6] In artificial systems, hydrogels, either derived from natural sources or synthetically made, are the preferred materials with which to mimic the ECM.[7,8] These materials simultaneously provide the water-based environment that is necessary to support cellular metabolism and the mechanical properties derived from the polymeric matrix,[9,10] and they are considered suitable for 3D culturing if, in addition to surviving, the behavior of the embedded cells is similar to that of the cells found in the native ECM. The desired behavior includes the characteristic elongation and migration of cells in environments susceptible to being metabolized and modified by them.[11] This aim of developing 3D systems promoting cell adhesion, which has motivated an extensive body of research over the last 20 years, stands in contrast with the needs of embryonic stem cells (ESCs).

As visibly represented in oviparous animals, ESCs develop as an independent system isolated from their surroundings; thus, cell-to-cell interaction is the sole driver of their development.[12] To mimic embryonic development *in vitro*, ESCs are aggregated in spheroids known as embryoid bodies (EBs), which are cultured in nonadherent environments, such as 3D-printed microaggregation devices,[13] conical plastic Aggrewell plates,[14] bioreactors,[15] and hanging drops.[16] However, the volume constraints of fixed-sized plastic wells, the limited time (i.e., three days) a drop of media can sustain an EB, and the lack of control in the bioreactors clearly indicate the insufficient development of tools for embryonic cultures in comparison to mature (i.e., differentiated) cells. However, when these EBs are grown in hydrogels suitable for the encapsulation of mature cells, either protein-based, such as gelatin,[17] or polysaccharides, such as chitosan,[18] stem cells rapidly lose their stemness and differentiate into various

Received: July 6, 2020
Revised: September 12, 2020
Published: September 15, 2020









https://dx.doi.org/10.1021/acs.biomac.0c01030
*Biomacromolecules* 2020, 21, 4814–4822

lineages. To prevent this spontaneous differentiation, stem cells cultured in 2D or 3D systems are forced to remain pluripotent by adding leukemia inhibitory factor (LIF) to the media, inhibiting differentiation and maintaining self-renewal.[19]

Nanocellulose is rapidly gaining relevance as a biocompatible material for tissue engineering and medical applications. Cellulose nanofibers (CNF) are cellulose fibrils with diameters of a few nanometers and lengths of several microns that are extracted from the cell walls of plants and microorganisms;[20−22] independently of the source, this material has strong intermolecular bonds that enable the formation of aqueous hydrogels for cell encapsulation.[23] The possibility of altering the physical and chemical properties of CNF hydrogels while preserving their biocompatibility has given rise to a handful of studies that have used them to encapsulate mammalian cells[24] or study their delivery.[25]

Here, we show how hydrogels based on cellulose nanofibers, a material that is exogenous to mammalian cells, can sustain the growth of ESCs for weeks, preserving their original differentiation potential without using differentiation inhibitors that hinder their natural development and enabling their enzymatic extraction from the 3D encapsulation. An initial batch of five CNF hydrogels with various degrees of oxidation was synthesized and analyzed mechanically for enzymatic degradation, as well as based on their ability to encapsulate and preserve a population of ESCs. Based on those results, the optimal degree of oxidation for the hydrogel was determined, and the ability to preserve pluripotency was subsequently studied. The results indicated that the pluripotency of the encapsulated cell is largely retained after two weeks in culture in the absence of LIF, in contrast with the findings from traditional 2D and 3D cultures in which ESC differentiation begins a few hours after chemical inhibition is removed. The results obtained indicate the potential of CNF as customizable hydrogels to maintain a population of ESCs dominated by their cell−cell interactions without hampering their stemness and while still preserving their viability in a physiological environment.

## METHODS

**Synthesis of Cellulose Hydrogel.** Cellulose slurry (plant source-derived cellulose nanofibers, 3 wt %) was obtained from Cellulose Lab (Fredericton, NB, Canada). The nonoxidized form of cellulose slurry was further optimized for various degrees of oxidation. Fifteen grams of the cellulose slurry was weighed, which accounts to 450 mg of the dry weight of cellulose. The slurry is dispersed finely in DI water (40 mL) followed by the addition of (2,2,6,6-tetramethylpiperidin-1-yl)oxyl (TEMPO) (7.6 mg,0.2 mmol) and NaBr (46.1 mg, 2 mmol). The entire setup is maintained in continuous stirring condition at room temperature (RT). The NaOCl solution (5% w/v, 20 mmol) was added dropwise, and the pH was maintained at 10.5 by adding 1 M NaOH solution until no more variation was observed. The five different types of CNF hydrogels (CNF1−CNF5) were formulated by altering the amount of the NaOCl added, ranging from low (CNF1) to high oxidation (CNF5). Finally, the prepared oxidized hydrogels were rinsed thoroughly with DI water until the pH reached 7.4. The hydrogels are then homogenized using an ultrasonic probe homogenizer (Fisherbrand 505, Fisher Scientific, Pittsburgh, USA) to 1% (w/v) concentration before using them for cell encapsulation.

**Rheological Characterization.** Rheological characterization was performed on all the formulated cellulose hydrogels using a hybrid rheometer (HR-2 Discovery, TA instruments, Delaware, USA) equipped with an environmental test chamber with a 20 mm diameter testing plate. All hydrogel samples were tested before and after incubation in culture medium for 24 h at 37 °C. Each sample was placed below the Peltier plate, and the shaft was lowered to maintain a working distance of 1600 $\mu$m. The excess hydrogel was squeezed out of the test plate and discarded. The tests were performed in triplicates, and averages and standard deviations were calculated. The storage modulus of the various cellulose hydrogel samples was measured at 2% strain, from 100 to 0.1 rad/s angular frequencies, and at 23 °C.

**FTIR.** Fourier transform infrared (FTIR) spectra of cellulose and dried cellulose hydrogel with various different oxidation degrees were obtained using an FTIR spectrometer (VERTEX 70 FTIR, Bruker Optik GmbH, Germany) with a resolution of 4 $cm^{-1}$ and accumulation of 1866 scans between 4000 and 400 $cm^{-1}$ on ATR mode. To avoid resonance overlapping with hydroxyl groups, the FTIR spectra of CNF were recorded in the acidic conditions used for transforming carboxylate to the carboxylic functional group.

**X-ray Diffraction.** X-ray diffraction patterns of all the TEMPO-oxidized cellulose nanofibers were obtained by using an XRD machine (D8 Discover, Bruker Optik GmbH, Germany). Nickel-filtered Cu K$\alpha$ radiation ($\lambda$ = 0.15418 nm) operated at 40 mA and 40 kV, with a scan speed of 3 $min^{-1}$, and 2$\theta$ ranging from 2 to 45°. The crystallinity indices (CI) were calculated as the height ratio between the intensity of the crystalline peak ($I_{002} - I_{am}$) and total intensity ($I_{002}$), where $I_{002}$ is the maximum intensity of 002 lattice diffraction, and $I_{am}$ is the intensity of the amorphous region at 2$\theta$ = 18°:

$$\mathrm{CI} = ((I_{002} - I_{am})/I_{002}) \times 100$$

**Determination of the Carboxylate Content.** The carboxylate content of all the TEMPO-oxidized cellulose nanofibers was determined by the electric conductivity titration method. A dried sample of the cellulose (approximately 50 mg) was mixed with 0.01 M HCl (15 mL) and DI water (20 mL). The mixture was stirred thoroughly to achieve a well-dispersed suspension. The samples were then titrated with a water solution of NaOH (0.5 M). The content of carboxylate groups was calculated using the equation

$$C = ((V_1 - V_0) \times (C_{NaOH}))/m$$

where $V_1$ and $V_0$ are the volumes of NaOH added before and after titration. $C_{NaOH}$ is the concentration of NaOH, and $m$ is the weight of the dried sample.

**Zeta Potential Measurements.** The zeta potential of 0.01% (w/v) of the TEMPO-oxidized cellulose nanofibers was determined using a zeta potential analyzer (Nanobrook Omni, Brookhaven Instruments, Holtsville, USA) at 25 °C. Each measurement was performed three times to calculate the average and the standard deviation.

**Scanning Electron Microscopy.** The formulated oxidized cellulose hydrogels along with the non-oxidized pure cellulose from the two different sources (i.e., commercial and coffee filter paper) were prepared using critical point drying using an increasing concentration of ethanol solutions for SEM analysis. The dehydrated samples were then gold-coated and analyzed using SEM (JSM-7600F, JEOL Ltd., Tokyo, Japan) at 10 kV.

**Cellulose Degradation Assay.** For the assessment of degradation, the cell-laden hydrogels were placed in a bath of cellulase enzyme from *Trichoderma reesei* (Sigma-Aldrich, Missouri, USA) in rocking conditions. The enzyme was diluted (150 $\mu$g/mg) in the same media used to support the encapsulated cells and was added to the 0.5 g of cellulose hydrogel placed on the bottom of a 24-well plate. Incubation was carried out at 37 °C, 5% $CO_2$. Every 5 h, the enzyme solution with the degraded cellulose was removed, the remaining solid mass of gel was weighted, and the fresh enzyme solution was added. The data of time-based degradation of the cellulose hydrogels was presented in a percentage degradation curve. The study was carried out in triplicates (Supplementary Figure S1).

**Cell Culture.** Before their encapsulation, embryonic stem cells R1/E (ATCC, Virginia, USA) were prepared in conditioning media composed by DMEM (Nacalai Tesque, Japan), 1% sodium pyruvate (Thermo Fisher Scientific, USA), 15% FBS (Gibco, USA), 1× nonessential amino acids (Thermo Fisher Scientific, Waltham, USA), 1% L-glutamax (Thermo Fisher Scientific, Waltham, USA), 0.1 mM 2-ß mercaptoethanol (Thermo Fisher Scientific, Waltham, USA), and


https://dx.doi.org/10.1021/acs.biomac.0c01030
Biomacromolecules 2020, 21, 4814−4822

1000 U/mL leukemia inhibitory factor (LIF) (Life Technologies, Carlsbad, USA). The cells were cultured on a gelatin-coated Petri plate (0.1%) (Sigma-Aldrich, St. Louis, USA) until confluency. The entire cell culture was performed at 37 °C and 5% $CO_2$. The culture media was renewed every alternate day. The cells were retrieved for experimentation by dissociating them using 0.25% trypsin−EDTA (Nacalai Tesque, Kyoto, Japan) and counted. The cell line was used in passage 18.

**EB Construction and Encapsulation.** The trypsinized cells were forced into embryoid bodies by the hanging drop method. Droplets of 20 $\mu$l of media with about 1000 cells per droplet were seeded on the lid of the Petri dish and left undisturbed for two days. The resulting cell aggregates were then injected into the cellulose hydrogel, avoiding the formation of air gaps. Hanging drops and the culture of the cell-laden hydrogels were performed using growth medium with a similar composition to the one used for cell culturing the ESCs but without LIF: DMEM, 1% sodium pyruvate, 15% FBS, 1× nonessential amino acids, 1% L-glutamax, and 0.1 mM 2-ß mercaptoethanol. The cell-laden hydrogels were maintained at 37 °C, 5% $CO_2$ and performed in triplicates with media replacements every 48 h. On days 3, 7, 11, and 15, the cell aggregates were extracted from the encapsulation using the cellulose degradation described above.

**3D Encapsulation in Alginate Hydrogel.** The trypsin-treated R1/E cells were used to form embryoid bodies by the hanging drop culture method. Each drop contained 1000 cells, which was incubated for two days. Post two days of incubation, the EBs were harvested and gently added to 3% sodium alginate solution. The EBs containing sodium alginate solution was gradually mixed and added to 0.5% $CaCl_2$ solution for gelation to occur. The EB−alginate solution was left undisturbed for 5 min. After the cross-linking process, all the $CaCl_2$ solution was drained out and replaced by cell culture medium. On day 7 and day 15, the cells were harvested from the 3D encapsulation to carry out cell sorting experiments. The alginate capsules with embedded EBs were treated with 10 mM EDTA solution for 5 min followed by centrifugation at 1000× g for 3 min to extract the EBs. These harvested EBs were then treated for flow cytometry analysis. We followed the previously reported protocol.[26]

**Optical Imaging and Cell Viability.** The LIVE/DEAD viability/cytotoxicity assay kit (Invitrogen, Carlsbad, USA) was added to the cells both in 3D culture and upon extraction onto 2D cell culture plates. The incubation was carried out for 30 min (for cells embedded in hydrogel) and 15 min (for cells postextraction) in the dark at 37 °C. The viability was indicated as green for live cells and red for dead cells and measured using an inverted microscope (AxioObserver Z1, Carl Zeiss, Germany). The experiments were performed in triplicates. Circularity was measured as radii dispersion by the minimum zone circle method.

For 3D imaging, the encapsulated cells were excited at 488/543 nm, and images were captured in the form of z-stack at an interval of 20 $\mu$m using a confocal laser scanning microscope (LSM-710, Carl Zeiss, Germany).

**Immunohistology.** The extracted EBs were stained for both pluripotency and cardiac differentiation. Post extraction at different time points the transferred EBs on the Petri dish were fixed with 4% paraformaldehyde for 15 min followed by permeabilization with 0.1% Triton X-100 (Nacalai Tesque, Kyoto, Japan). Blocking was carried with 5% BSA for 60 min at room temperature. Then, the blocked cells were incubated overnight at 4 °C with anti (OCT-4) and alpha sarcomeric actinin (1:200) (Life Technologies, Carlsbad, USA). The following day, the cells were incubated with secondary antibody conjugated with Alexa Fluor 546 (1:500) and Alexa Fluor 488 (1:500) (Life Technologies, Carlsbad, USA) for 60 min at room temperature. In the last step DAPI (4′,6-diamidino-2-phenylindole·2HCl) (1:1000) (Life Technologies, Carlsbad, USA) was added and maintained for 2 min. The cells were then imaged. All the steps described above were followed by a step consisting in three washes of 1X PBS for 5 min each. Imaging was performed using an inverted fluorescence microscope (AxioObserver Z1, Carl Zeiss, Germany). Fluorescence was quantified by calculating the ratio between the number of bright pixels from immunostaining and DAPI signals, as described previously.[27] A normalization between correlated images was performed using the background signals calculated on the void areas of the images. Due to the large datasets and to ensure the quality of the data, the tails of the distribution were removed by discarding the pixels with brightness more than one at one sigma of the mean brightness (i.e., remaining approximately 68% of the dataset).

**Flow Cytometry.** The pluripotency in different encapsulations after one week and 15 days was quantified by flow cytometry. Cells were cultured in the presence of LIF in 2D culture and not in the presence of LIF during EB formation stage and 3D culture (nonadherent CNF-2 and adherent alginate). Following the extractions and trypsinizations described above, cells were washed with 1X PBS, followed by fixation with 4% paraformaldehyde in rocking conditions for 10 min at room temperature. After incubation, the cell pellet was subsequently washed with 1X PBS and permeabilized with 0.1% Triton X-100. Following permeabilization, the cells were incubated with primary antibodies for 45 min, washed twice with 1X PBS, and finally incubated with a secondary antibody for another 45 min. For flow analysis, cells were washed for two times with PBS and resuspended in 1X PBS. The primary antibody used was anti-OCT-4 (1:200) (Life Technologies, Carlsbad, USA), and the secondary antibody used was Alexa Fluor 488 (1:500) (Life Technologies, Carlsbad, USA). The analysis was performed using a flow cytometer (MACSQuant Analyzer, Miltenyi Biotec, Bergisch Gladbach, Germany).

**Statistical Analysis.** All results were presented as the mean ± standard deviation. Statistical analysis was performed using a student's t-test or ANOVA in Microsoft Excel. Statistical significance was defined as $*p < 0.05$, $**p < 0.01$, and $***p < 0.001$. Three independent trials were carried out unless otherwise stated.

## RESULTS AND DISCUSSION

**Synthesis and Characterization of the Hydrogels.** The cellulose hydrogels were formulated by performing a TEMPO free radical oxidation reaction, as shown in Figure 1a. The free

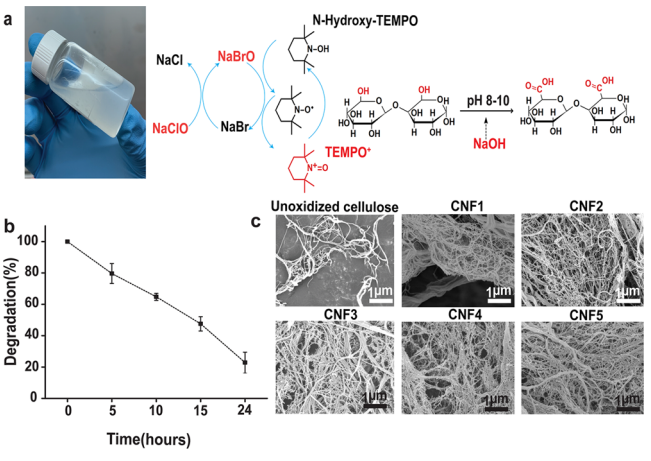


**Figure 1.** Characterization of all five CNF hydrogel systems. (a) Reaction mechanism that formulates the cellulose hydrogel through TEMPO-mediated surface reaction. (b) Enzymatic degradation of CNF2 (similar to CNF1) throughout 24 h and expressed as weight percentage loss. (c) Scanning electron microscopy of unoxidized and oxidized CNF from commercial sources. CNF1 being the least oxidized and CNF5 being the most TEMPO-oxidized hydrogel.

hydroxyl groups, which were made sterically available using a probe sonicator, were substituted by the carboxyl groups, resulting in a (1% w/v) transparent hydrogel from the commercial stock of cellulose slurry (3% w/v). Five types of hydrogels with an increasing degree of oxidation (CNF1−CNF5) were produced (Supplementary Figure S1). In addition


https://dx.doi.org/10.1021/acs.biomac.0c01030
Biomacromolecules 2020, 21, 4814−4822

to the correlation between oxidation degree and mechanical characteristics, we observed that the cellulosic hydrogels cross-linked with the glucose in the cell culture media, resulting in increased stiffness and resistance to enzymatic degradation (Figure 1b and Supplementary Figure S1). Therefore, the initial range of oxidations suitable for cell encapsulation was determined based on the characteristics of the CNF hydrogels postincubation in the cell culture media. The suitability of the hydrogels for degradation by cellulase seemed to be based on a threshold rather than continuous. The original five hydrogel types were divided between those that degraded and did so at similar rates (CNF1 and CNF2, Figure 1b) and those showing no degradation at all (CNF3−CNF5).

Two sources of plant cellulose fibers were initially tested for oxidation, the usual coffee filter cellulose and a standard commercial cellulose. While the morphological characteristics of the cellulose fibers obtained from the two sources were different in their native forms, those differences became negligible in their oxidized forms. The cellulose derived from coffee filters consisted of fibers 70−100 $\mu$m in diameter; which decreased from the range of 1 $\mu$m to a few nanometers postoxidation (Supplementary Figure S2). This observation agrees with the finding reported in the literature.[25] The diameter of the fibers in the commercial cellulose ranged from 100 to 1 $\mu$m in its native form, with no observable diameter changes after oxidation or between degrees of oxidation. This lack of correlation between the carboxylic content and fiber diameter has been reported previously in TEMPO-mediated oxidations of plant fibers.[28] Due to the morphological similitudes of the products from different sources and to ensure standardization, commercial cellulose was used for the remainder of the study.

The surface charge of the nanofibers was characterized as the zeta potential of the hydrogels.[29] As shown in Figure 2a, when the carboxylate content is 1.5 mmol/g, the zeta potential value recorded was −4.8 mV, but as the presence of the carboxylate group increases beyond 4 mmol/g, the value of the zeta potential becomes more negative (−13.86 mV). This measurement is indicative of the improved dispersion and stability of the more highly oxidized hydrogel in water. Interestingly, in tissue engineering, the negative values of the surface charge are associated with poor cell adhesion,[30] which could explain the nonadhesive nature of CNF hydrogels and the round morphology of the encapsulated cells.[25] The successful substitution of hydroxyl groups in the cellulose parent chain by carboxylic groups was monitored using Fourier transform infrared spectroscopy (FTIR) through the appearance of a peak at 1600 $cm^{-1}$, corresponding to the carbonyl stretching mode (Figure 2b). In agreement with previous observations[31] and despite the successful oxidation of the cellulose, no significant differences were observed on the crystallinity of different samples (Figure 2c), with all of them showing the characteristic cellulose I diffraction pattern with similar peaks at 15 (101) and 22° (002).[32] In contrast, the rheological characteristics of the hydrogels showed a strong correlation with the degree of oxidation (Figure 2d). The storage modulus of the minimally oxidized CNF1 was only slightly different from that of the raw material, while the mechanical strength[33] of the remainder of the samples was strongly influenced by oxidation degree. A more significant stiffening—and homogenization between samples—was observed when the hydrogels were exposed to the high glucose content of the cell culture media (Figure 2e). This phenomenon has been suggested to result from a physical cross-linking of the cellulose hydrogel in the presence of cell culture medium.[34]

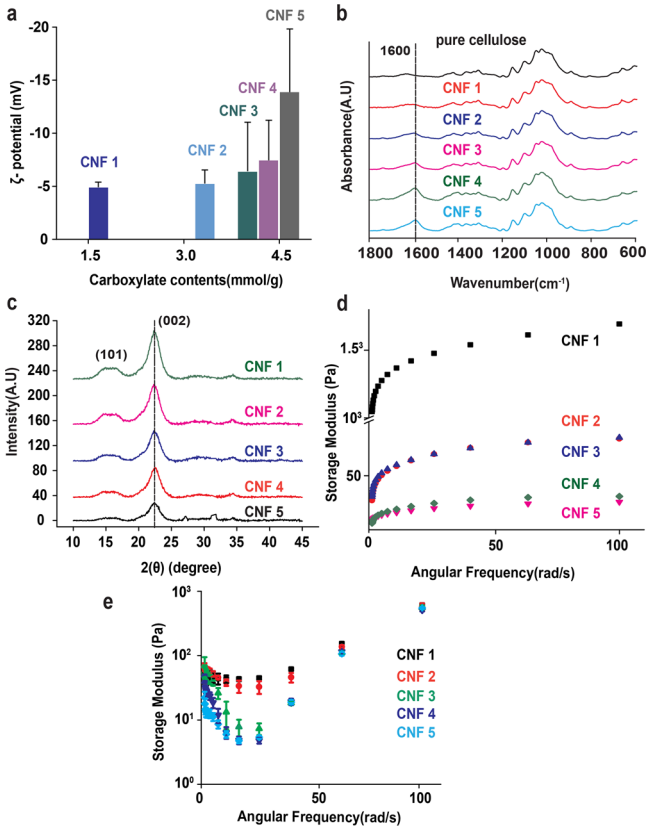


**Figure 2.** Characterization of CNF hydrogels. (a) Zeta potential values of all the five hydrogel systems with varying carboxylate content. (b) FTIR spectra of cellulose and CNF hydrogel. (c) X-ray diffractograms of CNF1−CNF5. (d) Storage modulus measurement for all the hydrogel types without the presence of cell culture medium. (e) Storage modulus measurement of all hydrogel types in the presence of cell culture medium.

**Formation of 3D Spheroids of mESCs in CNF Hydrogels.** The five CNF hydrogels were injected with EBs produced using the hanging drop culture method.[16] The CNF concentration (i.e., polymer to media) was fixed at 1% for all degrees of oxidation. Overall, similar growth was observed in all the cell populations and CNF hydrogel formulations. The biocompatibility of the 1% CNF hydrogels for mammalian cells has been studied previously;[35] however, our observations contradict the conclusion that 1% cellulose hydrogel is unable to host ESCs, and 0.5% is the optimal CNF concentration. This discrepancy is probably due to the different degrees of oxidation used and the influence of culture media in the properties of the CNF hydrogels, a phenomenon that was not considered in previous studies. During our biological experiments, we realized that while CNF hydrogels (0.1−1%) do not absorb light in the visible and ultraviolet (UV) range, they scatter incident light, thereby restricting brightfield observations. This limitation for white light microscopy can be easily circumvented using fluorescent microscopy. Interestingly, the low autofluorescence of CNF hydrogels[24] compared to other biopolymers used for cell encapsulation, e.g., fibronectin, collagen, or gelatin,[36] makes these hydrogels particularly suitable for the technique.

Over a period of two weeks, cell viability was indirectly observed via the continuous growth of EBs (Figure 3a and


https://dx.doi.org/10.1021/acs.biomac.0c01030
Biomacromolecules 2020, 21, 4814−4822

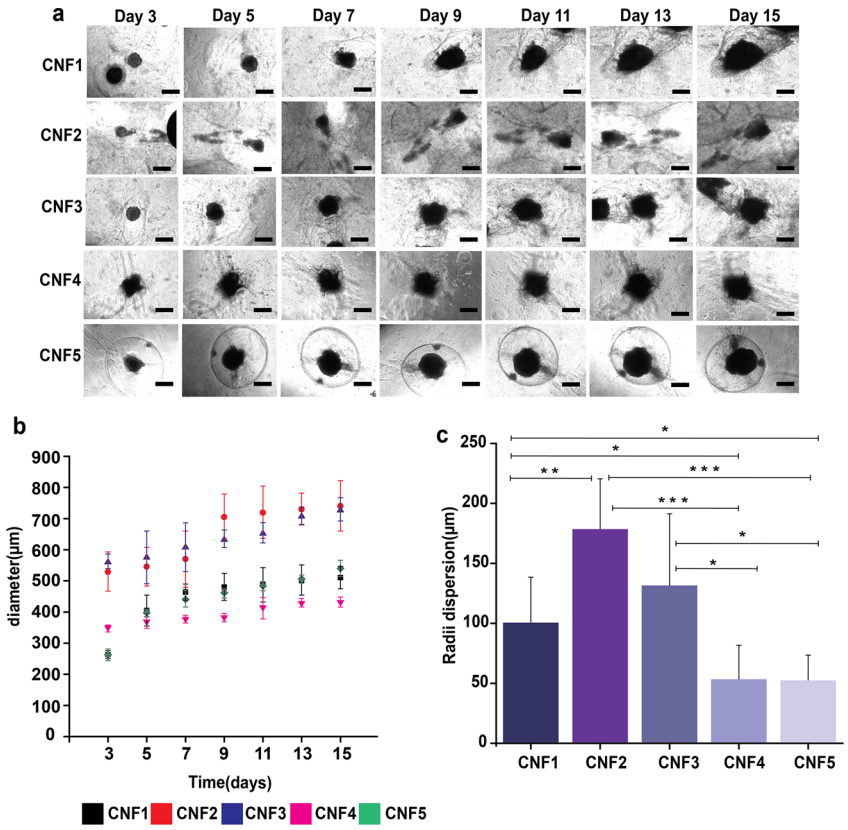


**Figure 3.** 3D cell encapsulation and characterization. (a) Embryoid body encapsulation in five hydrogel types and the enhancement in proliferation witnessed with an increase in incubation period (scale: 100 $\mu$m). (b) Statistically relevant increase in the diameter of the EBs over time. For each hydrogel system, the sample size considered was $n = 5$ with $p < 0.05$ for statistical significance. A more detailed comparison between each hydrogel type is presented in Supplementary Figures S4 and S5 (c) Roundness of the EBs calculated over two weeks. For each hydrogel system, the sample size considered was $n = 8$ with $p < 0.05$ for statistical relevance. The roundness of the EBs is quantified using the minimum zones circles method.

Supplementary Figure S3) and directly confirmed via cell staining. Overall, EB growth was observed in all five of the CNF hydrogels (Figure 3b). On day 3, the average EB diameters were 262.89 ± 13.3, 528.62 ± 64.3, 560.18 ± 26, 349.82 ± 14.2, and 262.63 ± 20.5 $\mu$m for CNF1−CNF5, respectively. Two weeks later, the diameters of the EBs had increased to 544.77 ± 41, 780.46 ± 72.11, 743.25 ± 70.5, 437.61 ± 37.77, and 553.58 ± 42.34 $\mu$m in the CNF1−CNF5 hydrogels, respectively (Supplementary Table S1). The inverse correlation between the degree of oxidation of the surrounding environment and the diameter of the EBs resulted from a higher packing density instead of slower growth (Supplementary Figures S4 and S5). As mentioned above, we believe this effect results from the increasingly negative surface charge of the environment (Figure 2a) rather than from the small differences in the mechanical characteristics after incubation (Figure 2e). At high degrees of oxidation, (i.e., CNF4 and CNF5) an enhanced roundness of the EBs was observed (Figure 3c, Supplementary Table S2), a property strongly linked to the survival of a developing embryo, because it is indicative of better cell compactness, improved conditions for proliferation, and a property linked to pluripotency.[37,38] These results are indicative of the better suitability of CNF4 and CNF5 to encapsulate EBs. However, their inability to be degraded enzymatically disqualifies them and CNF2 as viable platforms enabling the retrieval of the encapsulated population.

**Viability of 3D Spheroids in the CNF Hydrogels and Enzymatic Removal of the EBs.** To simulate the early development of an embryo, we encapsulated whole EBs rather than dissociated stem cells[39] into the system. This approach can be better correlated to an *in vivo* environment in which cell differentiation occurs in a highly organized fashion with a predetermined number of closely related cells.[40] Also, EBs selected to have similar cell number and diameter were injected in the five CNF hydrogels (Figure 4a), where they remained viable for the 15 days of the experiment (Supplementary Figures S7−S10). As a nonadhesive environment for mammalian cells, cellulose hydrogels promote EBs expanding their ECM[41] by enhancing the cadherin-mediated cell−cell interaction instead of cell−matrix interactions.[42,43] With the positive results from the cell viability/biocompatibility study, we moved forward to characterize the viable extraction of the EBs via the cellulase-catalyzed decomposition of those hydrogels that were susceptible to it (i.e., CNF1 and CNF2).

Cellulase derived from *Trichoderma reesei* was used to degrade the hydrogels and to extract the EBs on 2D platforms. Our preliminary results showed that a high degree of TEMPO oxidation (i.e., CNF3−CNF5) prevents the enzymatic degradation of the hydrogels at any feasible concentration. However, both CNF1 and CNF2 remained close enough to the native cellulose to be enzymatically degraded (Figure 4b). The specificity of the cellulase from *Trichoderma reesei* prevents its action on endogenous polysaccharides of the mammalian cell wall and ECM,[44,45] resulting in very selective degradation of the hydrogel matrix and the release of intact EBs. It has been reported previously that an enzymatic concentration of less than 300 $\mu$g/mg had a negligible effect on mammalian stem


https://dx.doi.org/10.1021/acs.biomac.0c01030
Biomacromolecules 2020, 21, 4814−4822

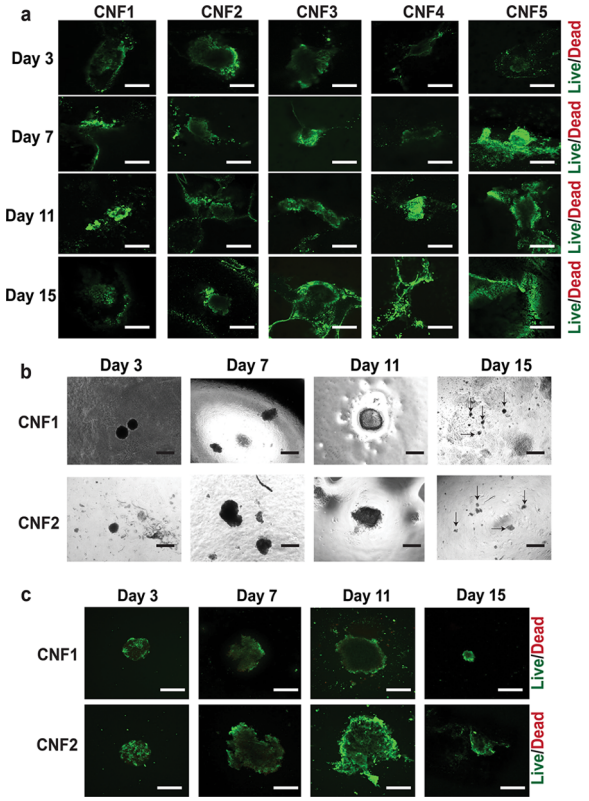


**Figure 4.** EB viability in 3D encapsulation and enzymatic treatment of cellulose hydrogel. (a) Confocal microscopy performed to study EB viability over the entire culture period of two weeks. EBs were encapsulated in CNF 1−5, and viability was checked at regular intervals. No dead cells were evidenced. Green indicates live cells stained by Calcein AM, and red represents dead cells stained by ethidium homodimer II (scale: 100 $\mu$m) (Supplementary Figure S6). Confocal 3D stack images are in the supplementary data (Supplementary Figures S7−S10). (b) Encapsulated EB released from CNF1 and CNF2 at regular intervals via the activity of cellulase (scale:100 $\mu$m). (c) Viability of the EBs after extraction from hydrogels susceptible to enzymatic degradation (CNF1 and CNF2). Hydrogels were degraded at regular intervals and stained with Calcein AM (green) and ethidium homodimer II (red). Some cell death is present on day 3, but cell death is absent later (scale :100 $\mu$m).

cells.[35] This extremum was not explored in our experiments, because an enzymatic concentration as low as 150 $\mu$g/mg successfully degraded CNF1 and CNF2. The now-free EBs were placed in culture plates to measure the extent of the damage due to the enzymatic extraction. The recovered EBs were treated with live/dead stain to confirm their viability. Interestingly, those EBs that were extracted from the CNF hydrogels during the first week (i.e., days 3 and 7) showed some degree of cell damage; however, no signs of impairment were observed at the later stages (i.e., days 11 and 15, Figure 4c, Supplementary Figure S6). This improved resistance to damage is probably because older EBs are more cohesive due to enhanced cell−cell cross-linking; therefore, they are better suited to withstand manipulation.

**Pluripotency of mESCs Extracted from CNF Hydrogels.** To determine the pluripotency of the mESCs in the formulated CNF hydrogels, we analyzed the octamer-binding transcription factor 4 (OCT-4) expressed by the stem cells. Remarkably, after one week of incubation in the hydrogels, the EBs remained fully pluripotent without significant variation in the OCT-4 expressed, as indicated by the fluorescence signal (Figure 5a,b). A drop in OCT-4 expression to about 55% of

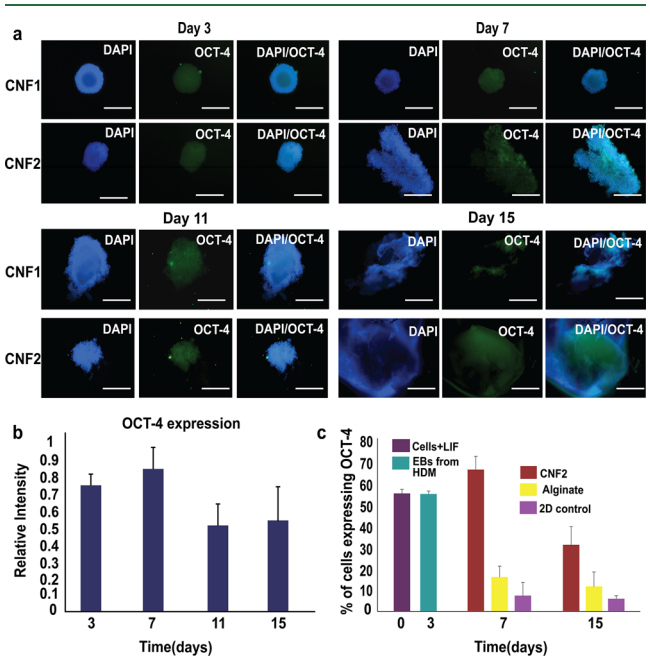


**Figure 5.** EB pluripotency after extraction. (a) Extracted EBs were also studied for pluripotency by staining them with an OCT-4 surface marker. Even after two weeks of incubation, the cells maintained their stemness. Green depicts OCT-4, and blue represents the nucleus (scale: 100 $\mu$m). (b) Pattern of expression for the OCT-4 surface protein marker in the encapsulated EBs over 15 days was measured as relative fluorescence intensity. (c) Flow cytometry analysis of the percentage of pluripotent cells in the encapsulated EBs on days 7 and 15, along with the values for a population maintained with LIF; EBs after recovery from a hanging drop; and an LIF-denied 2D control are represented (flow cytometry plots shown in Supplementary Figure S11). A 3D control experiment with an alginate hydrogel system is also represented (Supplementary Figure S12).

the initial value was observed a week postencapsulation; however, this level remained constant afterward. This result is noteworthy, because the EBs were cultured without using differentiation inhibitors (i.e., LIF). In these conditions, cells in traditional 3D and 2D cultures begin differentiating a few hours after implantation,[46] a process that is observable via a decrease in OCT-4 expression to about 10% by day 5 and negligible levels by day 7.[47] In contrast, the behavior and rate of differentiation in CNF hydrogels closely resembles that in mammalian embryos in which OCT-4 is downregulated only after day 8 of gestation during gastrulation but maintained later by its continuous expression in the primordial germ cells.[48] In CNF hydrogels, the downregulation of OCT-4 is observed between days 7 and 11 (Figure 5b), and similar to its expression pattern in early embryonic development, OCT-4 is maintained by half of the cells until at least 15 days in culture.

The OCT-4 expression in the stem cell population encapsulated in the optimal CNF hydrogels (i.e., CNF2) was independently measured using flow cytometry. These data were also compared to the expression of a similar mESC population growing in 2D cultures (i.e., tissue culture plate) and adhesive 3D cultures (i.e., alginate hydrogel). The result of the flow cytometry at days 7 and 15 (Figure 5c and Supplementary Figure S11) confirmed the aforementioned


https://dx.doi.org/10.1021/acs.biomac.0c01030
Biomacromolecules 2020, 21, 4814−4822

data based on fluorescence intensity, as well as previously reported observations in different platforms.

In the CNF platform proposed here, 69% of the LIF-denied cell population expressed measurable levels of OCT-4 after a week in culture, a value comparable to the original population. This value dropped to 31% of the population by day 15. This result is in stark contrast with the similar experiment performed in 2D tissue culture plates, where only 10 and 7% of the cells expressed measurable values of OCT-4 after one and two weeks in culture, respectively. Enhancing the cell−cell interaction by transitioning to an adherent 3D hydrogel improves those values. However, they remain one-third of those for the—also 3D but nonadherent—CNF hydrogel, with 20 and 10% of the cells expressing OCT-4 after one and two weeks in culture, respectively (Supplementary Figure S12).

Our observations are consistent with the established assumption that cell−cell interactions are the primary source of signaling in the *in vivo* development of an organism[49,50] and that therefore, they must define the paradigm of *in vitro* systems for embryonic development. This assumption is evident in the "natural" behavior shown in the *in vitro* system proposed in our study, resulting from a cohesive embryonic population prevented from establishing interactions other than those with adjacent cells. In these conditions, the EBs preserve their geometry and natural development; moreover, like *in vivo*, pluripotency is maintained by self-regulation, without external chemical stimulation.

## CONCLUSIONS

The holistic approach presented in this paper creates many opportunities to develop controlled environments and *in vitro* platforms, such as uterus-on-a-chip for the culturing and retrieval of embryonic populations at early stages of development. Diverging from the general biomedical approach of developing environments that are similar to the native ECM, we used a cellulose-based hydrogel system to provide a cohesive embryonic population with an isolated environment, one capable of supporting cell metabolism while protecting the cells from exogenous influences. Moreover, the hydrogel system can be modulated by changing the degree of oxidation to suit downstream applications. The proposed system, unique in its category, enables full control and observation of a cell population. Interestingly, in those conditions, we observed that recently formed EBs retain their pluripotency in a way that closely mimics the behavior found *in vivo*.

## ASSOCIATED CONTENT

### Supporting Information

The Supporting Information is available free of charge at https://pubs.acs.org/doi/10.1021/acs.biomac.0c01030.

Supplementary discussion on Oct-4, Nanog, and Sox-2; CNF formulation and enzyme degradation (Figure S1); CNF hydrogel derived from coffee paper (Figure S2); visualization of the encapsulated EBs inside the hydrogel (Figure S3); comparison of EB diameter dispersion for days 3 5, 7, and 9 (Figure S4); comparison of EB diameter dispersion for days 11, 13, 15, and 17 (Figure S5); quantification of the cell viability assay post extraction from hydrogel (Figure S6); 3D encapsulation of the cells on day 3 (Figure S7); 3D encapsulation of the cells on day 7 (Figure S8); 3D encapsulation of the cells on day 11 (Figure S9); 3D encapsulation of the cells on day 15 (Figure S10); quantitative analysis of the pluripotency of the stem cells by flow cytometry in the CNF hydrogel system (Figure S11); quantitative analysis of the pluripotency of the stem cells by flow cytometry in the alginate hydrogel system (Figure S12); embryoid body development characterization in terms of diameter (Table S1); embryoid body roundness dispersion in the hydrogel (Table S2) (PDF)

## AUTHOR INFORMATION


### Corresponding Author

**Javier G. Fernandez** − *Singapore University of Technology & Design, Singapore 487372 Singapore;* orcid.org/0000-0003-2961-6506; Email: javier.fernandez@sutd.edu.sg

### Author

**Rupambika Das** − *Singapore University of Technology & Design, Singapore 487372 Singapore*

Complete contact information is available at: https://pubs.acs.org/10.1021/acs.biomac.0c01030


### Author Contributions

R.D. and J.G.F.: conceptualization, methodology, and writing-original draft preparation. R.D.: data curation, experimentation, and image preparation. J.G.F.: supervision, reviewing, and editing.

### Notes

The authors declare no competing financial interest.

Data supporting the findings of this study are available within the article and its supplementary information files. Additional data and raw data are available from the corresponding author.

## ACKNOWLEDGMENTS

We thank Dr. Norris Ray Dunn (Lee Kong Chian School of Medicine, NTU) for his feedback. We also thank Dr. Naresh Sanandiya (SUTD, EPD) for passing on the knowledge of how to prepare cellulose-derived hydrogel in laboratory conditions. Special thanks to the Cellulose Lab, a company based in Canada who provided free samples of cellulose slurry to carry out our preliminary experiments. This work was partially supported by the National Research Foundation, Singapore (grant no. CRP20-2017-0004).

## REFERENCES


(1) Duval, K.; Grover, H.; Han, L.-H.; Mou, Y.; Pegoraro, A. F.; Fredberg, J.; Chen, Z. Modeling physiological events in 2D vs. 3D cell culture. *Physiology* **2017**, *32*, 266−277.

(2) Ravi, M.; Paramesh, V.; Kaviya, S. R.; Anuradha, E.; Solomon, F. D. P. 3D cell culture systems: advantages and applications. *J. Cell. Physiol.* **2015**, *230*, 16−26.

(3) Nicodemus, G. D.; Bryant, S. J. Cell encapsulation in biodegradable hydrogels for tissue engineering applications. *Tissue Eng., Part B* **2008**, *14*, 149−165.

(4) de Vos, P.; Lazarjani, H. A.; Poncelet, D.; Faas, M. M. Polymers in cell encapsulation from an enveloped cell perspective. *Adv. Drug Delivery Rev.* **2014**, *67-68*, 15−34.

(5) Frantz, C.; Stewart, K. M.; Weaver, V. M. The extracellular matrix at a glance. *J. Cell Sci.* **2010**, *123*, 4195−4200.

(6) Bowers, S. L. K.; Banerjee, I.; Baudino, T. A. The extracellular matrix: at the center of it all. *J. Mol. Cell. Cardiol.* **2010**, *48*, 474−482.

(7) Yang, Y.; Lu, Y. T.; Zeng, K.; Heinze, T.; Groth, T.; Zhang, K. Recent Progress on Cellulose-Based Ionic Compounds for Biomaterials. *Adv. Mater.* **2020**, 2000717.

(8) Park, M.; Lee, D.; Hyun, J. Nanocellulose-alginate hydrogel for cell encapsulation. *Carbohydr. Polym.* **2015**, *116*, 223−228.
(9) Vedadghavami, A.; Minooei, F.; Mohammadi, M. H.; Khetani, S.; Kolahchi, A. R.; Mashayekhan, S.; Sanati-Nezhad, A. Manufacturing of hydrogel biomaterials with controlled mechanical properties for tissue engineering applications. *Acta Biomater.* **2017**, *62*, 42−63.
(10) Fernandez, J. G.; Seetharam, S.; Ding, C.; Feliz, J.; Doherty, E.; Ingber, D. E. Direct Bonding of Chitosan Biomaterials to Tissues Using Transglutaminase for Surgical Repair or Device Implantation. *Tissue Engineering Part A* **2017**, *23*, 135−142.
(11) Shepard, J. A.; Huang, A.; Shikanov, A.; Shea, L. D. Balancing cell migration with matrix degradation enhances gene delivery to cells cultured three-dimensionally within hydrogels. *J. Controlled Release* **2010**, *146*, 128−135.
(12) Chen, S. S.; Fitzgerald, W.; Zimmerberg, J.; Kleinman, H. K.; Margolis, L. Cell-cell and cell-extracellular matrix interactions regulate embryonic stem cell differentiation. *Stem cells* **2007**, *25*, 553−561.
(13) Das, R.; Fernandez, J. G. Additive manufacturing enables production of de novo cardiomyocytes by controlling embryoid body aggregation. *Bioprinting* **2020**, No. e00091.
(14) Antonchuk, J. Formation of embryoid bodies from human pluripotent stem cells using AggreWell™ plates. In *Basic Cell Culture Protocols*; Springer: 2013, pp. 523−533.
(15) Kurosawa, H. Methods for inducing embryoid body formation: in vitro differentiation system of embryonic stem cells. *J. Biosci. Bioeng.* **2007**, *103*, 389−398.
(16) Wang, X.; Yang, P. In vitro differentiation of mouse embryonic stem (mES) cells using the hanging drop method. *JoVE (Journal of Visualized Experiments)* **2008**, *17*, No. e825.
(17) Ouyang, L.; Yao, R.; Mao, S.; Chen, X.; Na, J.; Sun, W. Three-dimensional bioprinting of embryonic stem cells directs highly uniform embryoid body formation. *Biofabrication* **2015**, *7*, No. 044101.
(18) Zhang, W.; Zhao, S.; Rao, W.; Snyder, J.; Choi, J. K.; Wang, J.; Khan, I. A.; Saleh, N. B.; Mohler, P. J.; Yu, J.; Hund, T. J.; Tang, C.; He, X. A novel core−shell microcapsule for encapsulation and 3D culture of embryonic stem cells. *J. Mater. Chem. B* **2013**, *1*, 1002−1009.
(19) Graf, U.; Casanova, E. A.; Cinelli, P. The Role of the Leukemia Inhibitory Factor (LIF) - Pathway in Derivation and Maintenance of Murine Pluripotent Stem Cells. *Genes (Basel)* **2011**, *2*, 280−297.
(20) Klemm, D.; Kramer, F.; Moritz, S.; Lindström, T.; Ankerfors, M.; Gray, D.; Dorris, A. Nanocelluloses: a new family of nature-based materials. *Angewandte Chemie International Edition* **2011**, *50*, 5438−5466.
(21) Torgbo, S.; Sukyai, P. Bacterial cellulose-based scaffold materials for bone tissue engineering. *Applied Materials Today* **2018**, *11*, 34−49.
(22) Andersson, J.; Stenhamre, H.; Bäckdahl, H.; Gatenholm, P. Behavior of human chondrocytes in engineered porous bacterial cellulose scaffolds. *Journal of biomedical materials research Part A* **2010**, *94*, 1124−1132.
(23) Pääkkö, M.; Ankerfors, M.; Kosonen, H.; Nykänen, A.; Ahola, S.; Österberg, M.; Ruokolainen, J.; Laine, J.; Larsson, P. T.; Ikkala, O.; Lindström, T. Enzymatic hydrolysis combined with mechanical shearing and high-pressure homogenization for nanoscale cellulose fibrils and strong gels. *Biomacromolecules* **2007**, *8*, 1934−1941.
(24) Bhattacharya, M.; Malinen, M. M.; Lauren, P.; Lou, Y.-R.; Kuisma, S. W.; Kanninen, L.; Lille, M.; Corlu, A.; GuGuen-Guillouzo, C.; Ikkala, O. Nanofibrillar cellulose hydrogel promotes three-dimensional liver cell culture. *J. Controlled Release* **2012**, *164*, 291−298.
(25) Sanandiya, N. D.; Vasudevan, J.; Das, R.; Lim, C. T.; Fernandez, J. G. Stimuli-responsive injectable cellulose thixogel for cell encapsulation. *Int. J. Biol. Macromol.* **2019**, *130*, 1009−1017.
(26) Horiguchi, I.; Sakai, Y. Alginate Encapsulation of Pluripotent Stem Cells Using a Co-axial Nozzle. *JoVE (Journal of Visualized Experiments)* **2015**, *101*, No. e52835.
(27) Waters, J. C. *Accuracy and precision in quantitative fluorescence microscopy*; The Rockefeller University Press: 2009.
(28) Serra, A.; González, I.; Oliver-Ortega, H.; Tarrés, Q.; Delgado-Aguilar, M.; Mutjé, P. Reducing the Amount of Catalyst in TEMPO-Oxidized Cellulose Nanofibers: Effect on Properties and Cost. *Polymer* **2017**, *9*, 557.
(29) Wei, J.; Chen, Y.; Liu, H.; Du, C.; Yu, H.; Ru, J.; Zhou, Z. Effect of surface charge content in the TEMPO-oxidized cellulose nanofibers on morphologies and properties of poly (N-isopropylacrylamide)-based composite hydrogels. *Industrial Crops and Products* **2016**, *92*, 227−235.
(30) McCune, D.; Guo, X.; Shi, T.; Stealey, S.; Antrobus, R.; Kaltchev, M.; Chen, J.; Kumpaty, S.; Hua, X.; Ren, W.; Zhang, W. Electrospinning pectin-based nanofibers: a parametric and cross-linker study. *Appl. Nanosci.* **2018**, *8*, 33−40.
(31) Saito, T.; Isogai, A. TEMPO-mediated oxidation of native cellulose. The effect of oxidation conditions on chemical and crystal structures of the water-insoluble fractions. *Biomacromolecules* **2004**, *5*, 1983−1989.
(32) Segal, L.; Creely, J. J.; Martin, A. E., Jr.; Conrad, C. M. An Empirical Method for Estimating the Degree of Crystallinity of Native Cellulose Using the X-Ray Diffractometer. *Text. Res. J.* **1959**, *29*, 786−794.
(33) Patel, A. R.; Dumlu, P.; Vermeir, L.; Lewille, B.; Lesaffer, A.; Dewettinck, K. Rheological characterization of gel-in-oil-in-gel type structured emulsions. *Food Hydrocolloids* **2015**, *46*, 84−92.
(34) Rashad, A.; Mustafa, K.; Heggset, E. B.; Syverud, K. Cytocompatibility of wood-derived cellulose nanofibril hydrogels with different surface chemistry. *Biomacromolecules* **2017**, *18*, 1238−1248.
(35) Lou, Y.-R.; Kanninen, L.; Kuisma, T.; Niklander, J.; Noon, L. A.; Burks, D.; Urtti, A.; Yliperttula, M. The use of nanofibrillar cellulose hydrogel as a flexible three-dimensional model to culture human pluripotent stem cells. *Stem cells and development* **2014**, *23*, 380−392.
(36) Jaafar, I. H.; LeBlon, C. E.; Wei, M.-T.; Ou-Yang, D.; Coulter, J. P.; Jedlicka, S. S. Improving fluorescence imaging of biological cells on biomedical polymers. *Acta Biomater.* **2011**, *7*, 1588−1598.
(37) Fierro-González, J. C.; White, M. D.; Silva, J. C.; Plachta, N. Cadherin-dependent filopodia control preimplantation embryo compaction. *Nat. Cell Biol.* **2013**, *15*, 1424−1433.
(38) Bongiorno, T.; Gura, J.; Talwar, P.; Chambers, D.; Young, K. M.; Arafat, D.; Wang, G.; Jackson-Holmes, E. L.; Qiu, P.; McDevitt, T. C.; Sulchek, T. Biophysical subsets of embryonic stem cells display distinct phenotypic and morphological signatures. *PLoS One* **2018**, *13*, No. e0192631.
(39) Malinen, M. M.; Kanninen, L. K.; Corlu, A.; Isoniemi, H. M.; Lou, Y.-R.; Yliperttula, M. L.; Urtti, A. O. Differentiation of liver progenitor cell line to functional organotypic cultures in 3D nanofibrillar cellulose and hyaluronan-gelatin hydrogels. *Biomaterials* **2014**, *35*, 5110−5121.
(40) Niakan, K. K.; Han, J.; Pedersen, R. A.; Simon, C.; Pera, R. A. R. Human pre-implantation embryo development. *Development* **2012**, *139*, 829−841.
(41) Azoidis, I.; Metcalfe, J.; Reynolds, J.; Keeton, S.; Hakki, S. S.; Sheard, J.; Widera, D. Three-dimensional cell culture of human mesenchymal stem cells in nanofibrillar cellulose hydrogels. *MRS Communications* **2017**, *7*, 458−465.
(42) Xu, Y.; Zhu, X.; Hahm, H. S.; Wei, W.; Hao, E.; Hayek, A.; Ding, S. Revealing a core signaling regulatory mechanism for pluripotent stem cell survival and self-renewal by small molecules. *Proceedings of the National Academy of Sciences* **2010**, *107*, 8129−8134.
(43) Li, L.; Bennett, S. A. L.; Wang, L. Role of E-cadherin and other cell adhesion molecules in survival and differentiation of human pluripotent stem cells. *Cell adhesion & migration* **2012**, *6*, 59−73.
(44) Suurnäkki, A.; Tenkanen, M.; Siika-aho, M.; Niku-Paavola, M.-L.; Viikari, L.; Buchert, J. Trichoderma reesei cellulases and their core domains in the hydrolysis and modification of chemical pulp. *Cellulose* **2000**, *7*, 189−209.


https://dx.doi.org/10.1021/acs.biomac.0c01030
*Biomacromolecules* 2020, 21, 4814−4822

(45) Tenkanen, M.; Puls, J.; Poutanen, K. Two major xylanases of Trichoderma reesei. *Enzyme Microb. Technol.* **1992**, *14*, 566−574.
(46) Pineda, E. T.; Nerem, R. M.; Ahsan, T. Differentiation patterns of embryonic stem cells in two-versus three-dimensional culture. *Cells Tissues Organs* **2013**, *197*, 399−410.
(47) Sajini, A. A.; Greder, L. V.; Dutton, J. R.; Slack, J. M. W. Loss of Oct4 expression during the development of murine embryoid bodies. *Dev. Biol.* **2012**, *371*, 170−179.
(48) Zeineddine, D.; Hammoud, A. A.; Mortada, M.; Boeuf, H. The Oct4 protein: more than a magic stemness marker. *Am J Stem Cells* **2014**, *3*, 74−82.
(49) Basson, M. A. Signaling in cell differentiation and morphogenesis. *Cold Spring Harbor Perspect. Biol.* **2012**, *4*, a008151.
(50) Watanabe, K.; Ueno, M.; Kamiya, D.; Nishiyama, A.; Matsumura, M.; Wataya, T.; Takahashi, J. B.; Nishikawa, S.; Nishikawa, S.-I.; Muguruma, K.; Sasai, Y. A ROCK inhibitor permits survival of dissociated human embryonic stem cells. *Nat. Biotechnol.* **2007**, *25*, 681−686.


https://dx.doi.org/10.1021/acs.biomac.0c01030
*Biomacromolecules* 2020, 21, 4814−4822